Current Alzheimer Research, 2021, *18*, 711-720

RESEARCH ARTICLE

Heterogeneity of Tau Deposition and Microvascular Involvement in MCI and AD

Annie G. Bryant[1], Mary K. Manhard[2], David H. Salat[2], Bruce R. Rosen[2], Bradley T. Hyman[1], Keith A. Johnson[1,2,3,4], Susie Huang[2,#], Rachel E. Bennett[1,#] and Yi-Fen Yen[1,*, #]

[1]*Department of Neurology, Harvard Medical School, MassGeneral Institute for Neurodegenerative Disease, Massachusetts General Hospital, Charlestown, MA, United States;* [2]*Department of Radiology, Massachusetts General Hospital, Athinoula A. Martinos Center for Biomedical Imaging, Charlestown, MA, United States;* [3]*Division of Nuclear Medicine and Molecular Imaging, Massachusetts General Hospital, Boston, MA, United States;* [4]*Center for Alzheimer Research and Treatment, Department of Neurology, Brigham and Women's Hospital, Boston, MA, United States*

Abstract: ***Background*:** Reduced cerebrovascular function and accumulation of tau pathology are key components of cognitive decline in Alzheimer's disease (AD). Recent multimodal neuroimaging studies show a correlation between cortical tau accumulation and reduced cerebral perfusion. However, animal models predict that tau exerts capillary-level changes that may not be fully captured by standard imaging protocols.

***Objective*:** Using newly-developed magnetic resonance imaging (MRI) technology to measure capillary-specific perfusion parameters, we examined a series of mild cognitive impairment (MCI) and AD patients with tau positron emission tomography (PET) to observe whole-brain capillary perfusion alterations and their association with tau deposition.

***Methods*:** Seven subjects with MCI or AD received Flortaucipir PET to measure tau deposition and spin-echo dynamic susceptibility contrast (SE-DSC) MRI to measure microvascular perfusion (<10μm radius vessels). Gradient-echo (GE) DSC and pseudocontinuous arterial spin labeling (P-CASL) MRI were also acquired to assess macrovascular perfusion. Tau PET, microvascular perfusion, and cortical thickness maps were visually inspected in volumetric slices and on cortical surface projections.

***Results*:** High tau PET signal was generally observed in the lateral temporal and parietal cortices, with uptake in the occipital cortex in one subject. Global blood flow measured by PCASL was reduced with increasing tau burden, which was consistent with previous studies. Tau accumulation was spatially associated with variable patterns of microvascular cerebral blood flow (CBF) and oxygen extraction fraction (OEF) in the cortex and with increased capillary transit heterogeneity (C-TH) in adjacent periventricular white matter, independent of amyloid-β status.

***Conclusion*:** Although macrovascular perfusion generally correlated with tau deposition at the whole-cortex level, regional changes in microvascular perfusion were not uniformly associated with either tau pathology or cortical atrophy. This work highlights the heterogeneity of AD-related brain changes and the challenges of implementing therapeutic interventions to improve cerebrovascular function.

ARTICLE HISTORY

Received: April 13, 2021
Revised: June 10, 2021
Accepted: August 28, 2021

DOI:
10.2174/1567205018666211126113904

Keywords: Alzheimer's disease, tau pathology, microvascular perfusion, multimodal neuroimaging, positron emission tomography, dynamic susceptibility contrast magnetic resonance imaging, cerebrovascular function.

1. INTRODUCTION

Vascular dysfunction and tau neurofibrillary tangle (NFT) formation are key contributors to the Alzheimer's disease (AD) neuropathological cascade. Broadly, reduced cerebral perfusion is known to occur early in the disease course, before the onset of frank neurodegeneration or detectable changes in metabolism on fluorodeoxyglucose (FDG)-positron emission tomography (PET) [1-3]. While *in vivo* tau pathology correlates well with cognitive decline [4-9], the functional relationship between pathological tau deposition and diminished vascular function in the human cortex remains uncertain. Recent preclinical findings in transgenic mice suggest that tau pathology drives neurovascular uncoupling [10], alterations to microvascular structure [11], and impaired capillary flow *via* transient leukocyte adhesion [11]. Such leukocyte-perturbed capillary flow patterns are a

* Address correspondence to this author at the Department of Radiology, Faculty of the Athinoula A. Martinos Center for Biomedical Imaging, Massachusetts General Hospital, Bldg. 149, 13th Street, Charlestown, Massachusetts, USA; Tel: 617-726-4060; E-mail: yyen1@mgh.harvard.edu
#*These authors contributed equally to this work.*

1875-5828/21

phenocopy of those reported in the human traumatic brain injury literature [12, 13], and they may reflect cortical capillary transit heterogeneity (CTH) previously described in human AD [14-16].

Human neuroimaging studies have demonstrated localized inverse correlations between increased tau burden and reduced macrovascular cerebral blood flow (CBF) *in vivo* across the cognitive spectrum [17-20]. However, both tau pathology [21, 22] and vascular function [23] exhibit pronounced spatiotemporal variability *in vivo*, suggesting the existence of distinct tau and vascular pathology subtypes. Examining whole-brain tau and cerebrovascular function distributions could elucidate important regional associations at the individual level. Moreover, while CBF is an integral component of functional neurovascular coupling, changes in CTH and oxygen extraction fraction (OEF) levels can reflect microvascular dysfunction even with supra-ischemic CBF levels [16]. Indeed, Jespersen and Østergaard [24] propose that the combined effects of CBF, CTH, and OEF better capture cerebral hemodynamics than those of CBF alone. It is thus relevant to examine tau-related CBF in the context of these other microvascular biomarkers, which reflect capillary dysfunction and are associated with cognitive decline and neurodegeneration in AD [14, 15, 25].

Based on mounting preclinical and clinical evidence, we hypothesized that a high regional tau burden would spatially colocalize with low microvascular CBF and high microvascular CTH in the cortex. Here, we sought to characterize microvascular perfusion using spin-echo dynamic susceptibility contrast (SE-DSC) magnetic resonance imaging (MRI), which is particularly sensitive to susceptibility contrast signal in small vessels such as capillaries (radius < 10 μm) [26, 27] and from which CBF, CTH, and OEF parametric maps can be derived. Microvascular perfusion maps are visualized along with tau PET imaging in seven cognitively impaired subjects to examine qualitative spatial associations. To compare our data with previously published studies [17-20], we also acquired gradient echo DSC (GE-DSC) MRI and pseudocontinuous arterial spin labeling (PCASL), which measure perfusion signals from vessels of all sizes, from capillaries to large arteries.

2. MATERIALS AND METHODS

2.1. Subjects

This study was approved by the Institutional Review Board of Mass General Brigham and was HIPAA compliant. Seven subjects previously diagnosed with MCI (n=6) or AD (n=1) and with prior amyloid-β and tau PET scans were recruited to undergo SE-DSC, GE-DSC, and PCASL MRI at the Massachusetts General Hospital (MGH). In addition, cognitive status was assessed using the Mini-Mental State Examination (MMSE) [28], Clinical Dementia Rating (CDR) Global score [29], Sum of Boxes (SoB) [30], and the Montreal Cognitive Assessment (MoCA) [31].

2.2. Image Acquisition and Processing

Anatomical MRI was acquired with 1mm isotropic T1-weighted magnetization-prepared rapid acquisition with gradient echo (MPRAGE) and T2-weighted fluid-attenuated inversion recovery (FLAIR). Amyloid-β plaque deposition was measured using Pittsburgh Compound-B (PiB) PET and tau NFT burden was measured using Flortaucipir ([^{18}F]-AV-1451) PET, with standardized uptake value (SUV) maps generated as previously described [32]. A novel dual-echo SE-DSC and GE-DSC MRI sequence [33] was acquired with intravenous injection of 0.1 mmol/kg gadolinium-based contrast agent using the following parameters: 2.4mm in-plane resolution, 33 3mm-thick slices, 15% slice gap; repetition time (TR) 1500ms, echo time (TE) 90ms; 244 time series with temporal resolution 1.5s. SE-DSC and GE-DSC time-series data were processed using pgui (PGUI Perfusion Analysis Software; Center of Functionally Integrative Neuroscience, Aarhus University Hospital Norrebrogade, Denmark; https://cfin.au.dk/software/pgui/) to yield parametric maps, including CBF, CTH, and oxygen extraction fraction (OEF).

Multi-band PCASL [34] was acquired using a 3T MRI scanner (Magnetom Prisma, Siemens, Munich, Germany) and a Siemens 32-channel head coil. Labeled and control images were collected at the following post-label delay intervals: 0.2s (n=12 measurements), 0.7s (n=12 measurements), 1.2s (n=12 measurements), 1.7s (n=20 measurements), 2.2s (n=30 measurements). At each post-label delay, 60 2.27mm-thick slices were acquired with TR 8000ms and TE 40ms. Motion correction was performed using *3dvolreg* from Analysis of Functional NeuroImages (AFNI) [35], using the median frame in the time-series as the template volume for co-registration. Perfusion was quantified using the *oxford_asl* script from the Bayesian Inference for Arterial Spin Labeling MRI (BASIL) toolbox [36].

Image registration and segmentation were performed using FreeSurfer 7.1.1 (https://surfer.nmr.mgh.harvard.edu/). The PET SUV and perfusion parametric maps were registered to anatomical MRI and normalized to the mean cerebellum cortex and sensorimotor cortex, respectively, yielding relative maps (denoted with, *e.g.*, "SUVR" or "rCBF"). The sensorimotor cortex was selected as a perfusion reference region given its relative sparing in AD pathology and previous usage for perfusion quantification in the AD brain [37-43]. Additionally, the PiB PET distribution volume ratio (DVR) was calculated for a large cortical ROI encompassing frontal, lateral temporal, and retrosplenial cortices (FLR) following partial volume correction as described previously [32]. Amyloid-β positivity was defined as an FLR PiB DVR of 1.3 or greater [44-46]. All co-registered functional maps were brain-masked and spatially smoothed with a 6mm Gaussian kernel using FreeSurfer. To complement visualization in subject space, each subject's structural and functional volumes were registered to a group-averaged template using combined volumetric and surface registration [47, 48]. Volumetric data were additionally projected onto the template

cortical surface with even sampling between the white and pial surfaces using FreeSurfer.

2.3. Image Visualization and Analysis

Volumetric slice and functional overlay visualizations were generated using the *oro.nifti* and *neurobase* packages in R. The inflated template cortical surface was flattened by first introducing relaxation cuts (see https://surfer.nmr.mgh.harvard.edu/fswiki/FreeSurferOccipitalFlattenedPatch) and using FreeSurfer's surface flattening tool. Functional data projected onto the surface were visualized on the template cortical flatmap using pycortex [49] in python (v3.8).

2.4. Statistical

Vertex-wise cortical surface summary statistics were calculated for cortical thickness, SE rCBF, GE rCBF, PCASL rCBF, and tau SUVR for each subject using the *freesurferformats* package in R (v4.0.2). Pearson's product moment correlation coefficient (r) and p-values were calculated using the cor.test() function from the *stats* package in R.

3. RESULTS

3.1. Subject Information

Seven subjects (6 MCI/1 AD, mean age 76.7 ± 6.7) underwent PET and MRI, with an average of 2.7 ± 1.2 years in between PET and perfusion MRI scans. Subject demographics, cognitive scores, amyloid-β status, and APOE genotypes are shown in Table **1**. All subjects met National Institute on Aging-Alzheimer's Association criteria for cognitive impairment, with n=6 MCI (CDR global score of 0.5) [50] and n=1 AD (CDR global score of 1) [51]. Additionally, based on CDR SoB scores, these subjects exhibited either questionable cognitive impairment (n=5), very mild dementia (n=1), or mild dementia (n=1) [30].

Table **2** shows the whole-cortex tau SUVR mean and standard deviation for each subject, with a mean cortical tau SUVR of 1.22 ± 0.31 across the seven subjects. Five subjects exhibited PiB FLR DVR > 1.3 and were therefore classified as amyloid-β positive (Table **1**). The two amyloid-β negative subjects (Sub06 and Sub07) exhibited relatively low cortical tau SUVR compared to other subjects (Fig. **1**), with cortical accumulation limited to the medial temporal region. This pattern of medial temporal tau deposition, coupled with mild cognitive impairment, suggests primary age-related tauopathy (PART) [52], though other neuropathologies such as Lewy body disease and major depressive disorder cannot be ruled out. Three subjects had at least one APOE ε4 allele (Sub01, Sub03, Sub05), two subjects had ε3/ε3 (Sub06, Sub07), and two subjects did not have APOE genotype data available (Sub02, Sub04).

3.2. PCASL-Measured Blood Flow Reflects Whole-Cortex Tau Deposition

Previous studies indicate that global cortical CBF is reduced in AD [53-57]. To compare these subjects with previous work, we first obtained values for whole-cortex cerebral blood flow as measured by each of the three rCBF sequences: SE, GE, and PCASL (Table **2**). PCASL-derived rCBF exhibited a significant negative correlation with tau SUVR at the whole-cortex level ($r = -0.790$, $p = 0.035$), which is in line with previous studies showing negative associations at the regional level [17, 18, 20]. Neither SE-rCBF nor GE-rCBF correlated with tau SUVR at the whole-cortex level. Average cortical thickness was also comparable across subjects and did not correlate with tau, although the one AD subject (Sub01) did have the second-greatest cortical tau SUVR (1.40) and the lowest average cortical thickness (1.99 mm).

3.3. Tau Deposition and Microvascular Perfusion Exhibit Intra-Subject Spatial Variability

To provide an overview of tau NFT distribution throughout the cortex and subcortical structures in these seven subjects, representative coronal slices are shown in group-average template space in Fig. (**1**). Individual patterns of tau deposition varied by subject and did not clearly adhere to strict Braak staging schemes [58, 59]. Consistent with AD-susceptible brain areas, the highest cortical tau SUVR was generally observed in the middle and inferior temporal regions, though Sub01 showed high occipital cortex uptake and Sub03 showed high frontal, parietal, and cingulate uptake. Of note, most subjects also exhibited clear asymmetries, with one hemisphere showing greater overall tau burden.

Next, we examined the microvascular (SE-DSC) perfusion maps from these subjects to see if local areas of altered capillary rCBF matched areas of high tau deposition. Representative structural FLAIR, tau-PET, and SE-DSC parametric maps are shown in volumetric slices in Fig. (**2**). We compared areas of asymmetric tau uptake (circled) to the contralateral hemisphere and surrounding parenchyma and examined the relationships with rCBF, rCTH, and rOEF. Among the amyloid-positive subjects (Sub01, Sub02, Sub03, Sub04, Sub05), most had at least one high-tau region that overlapped with reduced rCBF, though there were notable exceptions in which the relationship between tau uptake and rCBF was more heterogeneous. For example, Sub03 (Fig. **2C**; 66F, CDR SoB 2) exhibited higher tau burden throughout the right parietal, temporal, and cingulate cortices compared with the left hemisphere, with many areas of elevated tau uptake corresponding to relatively higher rCBF and lower rOEF. By contrast, the amyloid-negative subjects - Sub06 (Fig. **2F**; 82M, CDR SoB 3) and Sub07 (Fig. **2G**; 79F, CDR SoB 1) - exhibited lower rCBF within areas of elevated tau but higher rCBF in the surrounding brain parenchyma.

High rCTH was also observed in cortical regions and, unexpectedly, in periventricular white matter adjacent to areas of elevated tau uptake. For example, Sub04 (Fig. **2D**; 70M, CDR SoB 2.5) had a focus of elevated tau uptake in the right inferior parietal cortex, with high rCTH in the subjacent periventricular white matter. Sub06 (Fig. **2F**) showed mild tau deposition in the right entorhinal cortex, which also

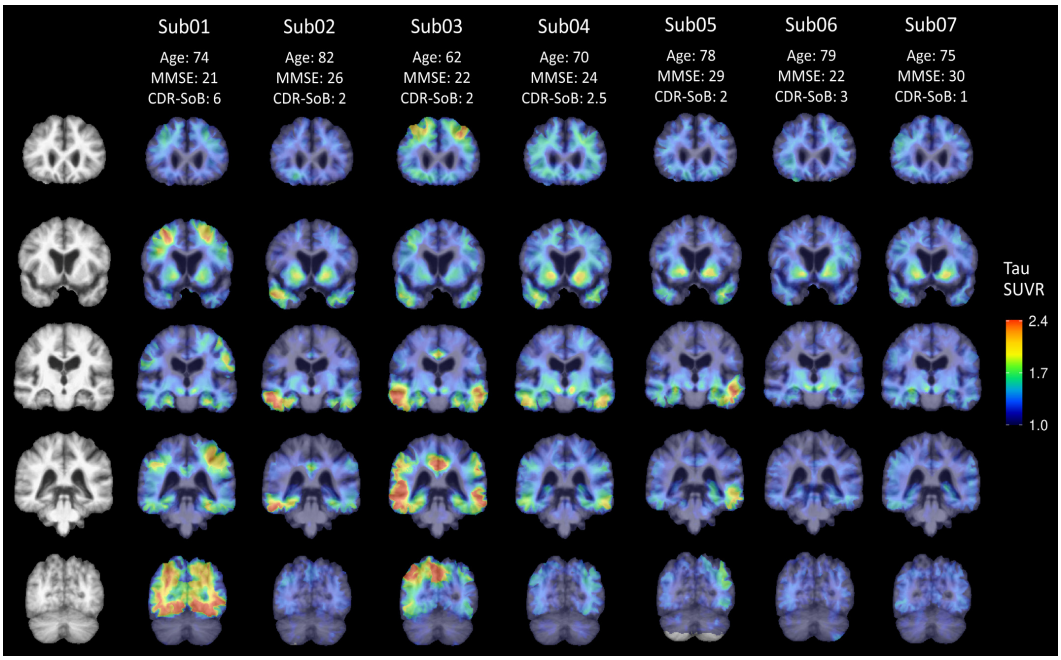

Fig. (1). Tau SUVR overlaid on the group-average template structural MRI slices at coronal levels that demonstrate tracer distribution in each case. *(A higher resolution / colour version of this figure is available in the electronic copy of the article).*

Table 1. Demographic and cognitive information for the subjects in this case series study. Amyloid-β positivity is defined as a partial volume corrected FLR (frontal, lateral temporal, and retrosplenial cortex) distribution volume ratio (DVR) of 1.3 or greater. Summary statistics in the final row are presented as mean (standard deviation).

Subject	Diagnosis	Age at Tau Scan	Sex	MMSE	CDR SoB	CDR Global	Years between Tau/MRI	APOE	Amyloid-β
Sub01	AD	74	F	21	6	1	2.9	e3/e4	+
Sub02	MCI	82	M	26	2	0.5	2.9	NA	+
Sub03	MCI	62	F	22	2	0.5	3.8	e4/e4	+
Sub04	MCI	70	M	24	2.5	0.5	0.5	NA	+
Sub05	MCI	78	M	29	2	0.5	1.7	e3/e4	+
Sub06	MCI	79	M	22	3	0.5	3.2	e3/e3	-
Sub07	MCI	75	F	30	1	0.5	4.1	e3/e3	-
n=7	6 MCI, 1 AD	74.3 (6.7)	4M, 3F	24.9 (3.6)	2.6 (1.6)	6 $CDR_{0.5}$, 1 CDR_{1}	2.7 (1.2)	3 $e4^{+}$, 2 $e4^{-}$, 2 NA	5+, 2-

Table 2. Summary statistics from functional data projected onto the cortical surface in individual subject space. Values are presented as the mean (standard deviation) across all cortical surface vertices per subject. In the bottom row, results from Pearson's correlation test are shown for each column compared with Tau SUVR across the seven subjects. a.u. = arbitrary units.

Subject	Cortical Thickness (mm)	SE rCBF (a.u.)	GE rCBF (a.u.)	PCASL rCBF (a.u.)	Tau SUVR (a.u.)
Sub01	2.19 (0.59)	0.82 (0.33)	0.67 (0.35)	0.62 (0.35)	1.38 (0.41)
Sub02	2.17 (0.57)	0.79 (0.33)	0.71 (0.43)	0.81 (0.38)	1.13 (0.28)
Sub03	2.26 (0.49)	0.74 (0.43)	0.82 (0.61)	0.67 (0.22)	1.43 (0.40)
Sub04	2.38 (0.48)	0.71 (0.27)	0.80 (0.66)	0.64 (0.20)	1.24 (0.25)
Sub05	2.25 (0.53)	0.61 (0.23)	0.69 (0.57)	0.78 (0.33)	1.14 (0.26)
Sub06	2.29 (0.47)	0.91 (0.34)	0.82 (0.53)	0.78 (0.30)	1.10 (0.20)
Sub07	2.38 (0.56)	0.88 (0.37)	0.77 (0.65)	0.70 (0.22)	1.15 (0.20)
Correlation with Tau SUVR	r = -0.188 p = 0.687	r = -0.173 p = 0.709	r = 0.075 p = 0.872	r = -0.790 p = 0.035	-

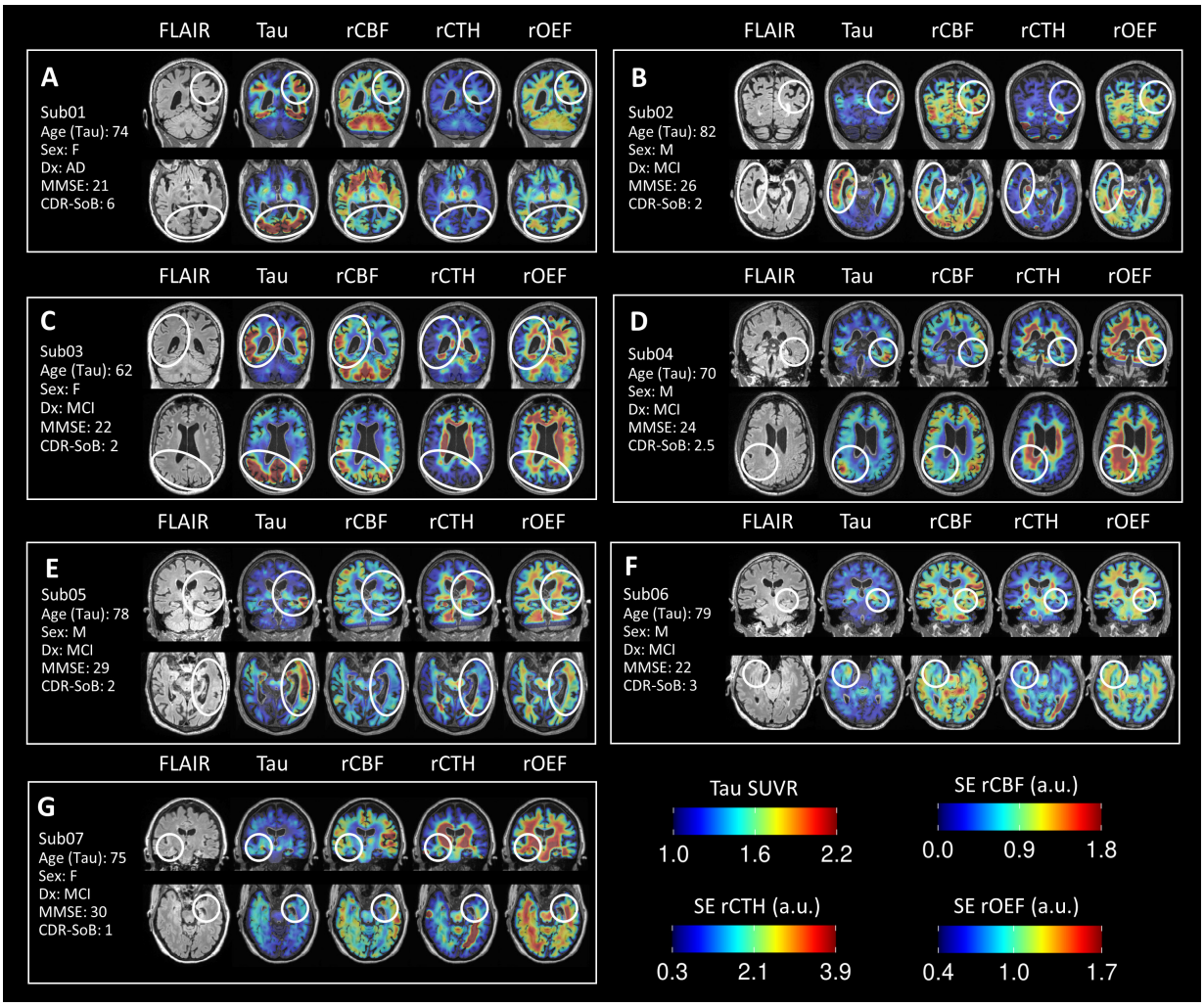

Fig. (2). Representative slices showing FLAIR, tau-PET SUVR, rCBF, rCTH, and rOEF parametric maps for each subject. All volumes are presented in individual subject space. White ovals highlight regions with high tau-PET signal and/or noteworthy SE-DSC microvascular patterns. a.u. = arbitrary units. *(A higher resolution / colour version of this figure is available in the electronic copy of the article).*

exhibited high rCTH and low rCBF. Sub05 (Figs. **2E**; 79M, CDR SoB 2) showed asymmetrically high tau deposition in the left middle temporal cortex and amygdala, which collectively exhibited diminished rCBF compared with the right hemispheric counterparts and markedly higher rCTH and rOEF in the adjacent periventricular white matter. While all subjects exhibit variably increased rCTH in the periventricular white matter (notably Figs. **2C**, **D**, **E**, and **G**), such increased rCTH only coincided with FLAIR signal hyperintensity in Sub02 (Fig. **2B**), with no FLAIR signal abnormalities detected in the other subjects.

3.4. Tau Deposition and Microvascular Function Exhibit Heterogeneity on the Cortical Surface

To assess the relationship between tau uptake and microvascular perfusion parameters across subjects, maps of tau uptake, perfusion parameters, and cortical thickness were projected onto a group-averaged cortical surface flatmap (Fig. **3**). This enabled the investigation of spatial associations between cortical tau pathology, microvascular function, and atrophy within the same group-averaged space. A flatmap atlas is included in Fig. (**S1**) for guidance. Despite relatively consistent spatial patterns in cortical thickness, the tau SUVR and rCBF maps differed markedly across subjects. For example, Sub01 and Sub03 had the most cortical tau deposition among all subjects, yet rCBF in Sub01 was uniformly diminished in areas of elevated tau uptake, while rCBF in Sub03 was preserved to elevated in areas of increased tau and adjacent regions. Sub02 and Sub06 showed marked asymmetry between cerebral hemispheres in tau deposition, with areas of lower rCBF corresponding to areas of greater tau uptake. In other subjects, the relationship between tau uptake and rCBF was more complex. For example, Sub03 and Sub07 showed fairly symmetric tau burden between cerebral hemispheres and asymmetric patterns of

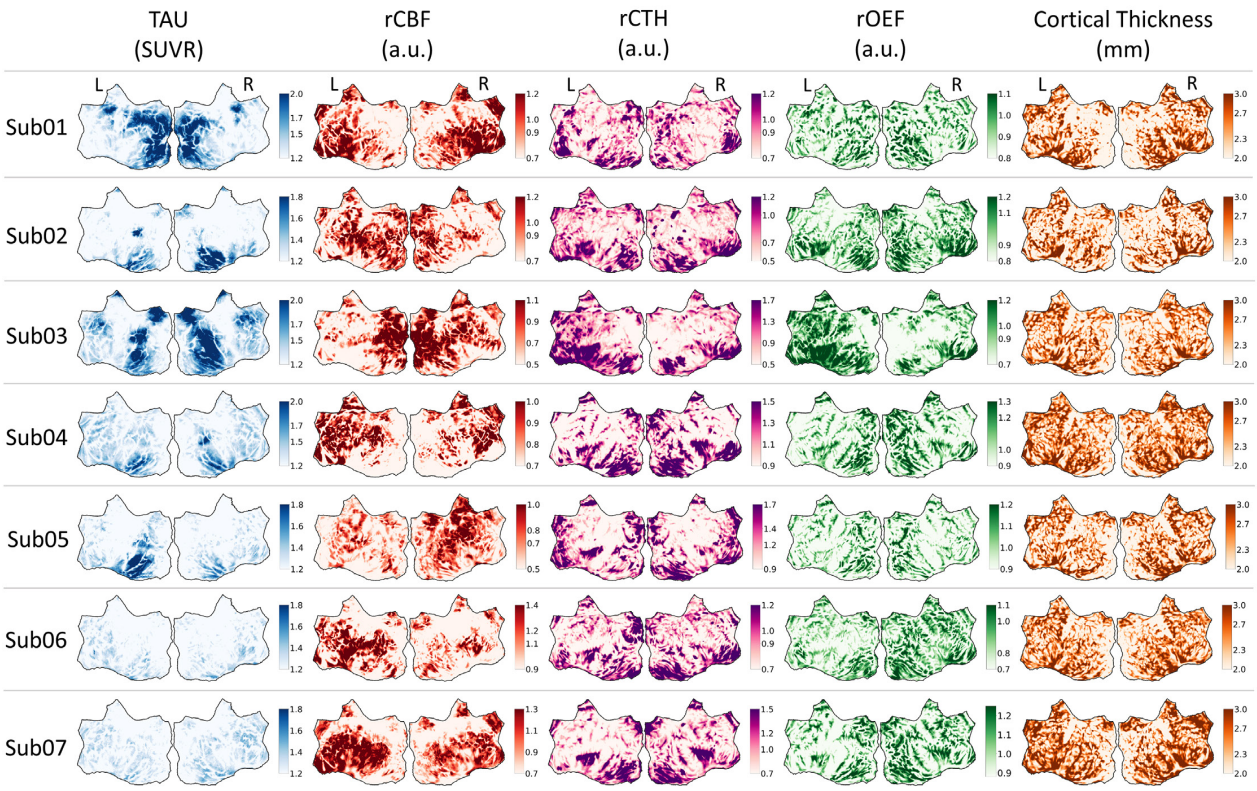

Fig. (3). Tau-PET SUVR, rCBF, rCTH, rOEF, and cortical thickness surface data projected onto the flattened group-average template surface. Left and right hemispheres are indicated with L and R, respectively. a.u. = arbitrary units. *(A higher resolution / colour version of this figure is available in the electronic copy of the article).*

rCBF, including higher rCBF in the right cerebral hemisphere in Sub03 that appeared to correspond to slightly greater tau uptake in the same hemisphere. While greater rCBF in one hemisphere often showed asymmetrically lower rOEF and/or rCTH in the same hemisphere, as exemplified in Sub06, this trend was not universal, with Sub05 showing symmetric rCTH and rOEF maps despite focally elevated rCBF in the right cerebral hemisphere.

4. DISCUSSION

Based on the growing literature documenting associations between high tau burden and reduced blood flow in the cortex, we hypothesized that tau deposition would be spatially associated with low rCBF in these seven cognitively impaired subjects. We additionally hypothesized that tau burden would be associated with high rCTH, given evidence of tau-driven capillary flow heterogeneity in the murine cortex [11]. While we observed a negative association between tau burden and PCASL CBF at the whole-cortex level, the visualizations provided herein indicate that the relationship between tau pathology is more nuanced. Given the relative consistency of cortical thickness distribution across these seven subjects, it is not likely that such microvascular heterogeneity is driven by cortical atrophy alone but rather by complex underlying physiology.

Spatiotemporal variability in tau pathology is increasingly recognized as the norm rather than the exception [21, 22, 60], underscoring the need to examine whole-brain tau and vascular dynamics at the individual patient level. The microvascular heterogeneity observed in our cohort may be driven in part by variability in individual tau pathology trajectory, though future longitudinal analysis is needed to clarify such a mechanism. The observed microvascular asymmetry between hemispheres also warrants further study, as it may relate to “misery perfusion”, a phenomenon in which reduced CBF in one hemisphere induces elevated OEF compared with the contralateral hemisphere. Misery perfusion has been reported in various cerebrovascular pathologies [61, 62] as well as in AD [63].

In addition to a variable pattern of cortical perfusion, we also observed high rCTH in the periventricular white matter in several subjects. Several areas of elevated rCTH appeared in the periventricular white matter subjacent to areas of elevated tau uptake, suggesting the alteration of microvascular dynamics in white matter in association with cortical tau pathology. Such areas of elevated rCTH were primarily ob-

served in the absence of white matter lesions on FLAIR imaging, which are the expected hallmark of cerebrovascular damage in small vessel disease [64, 65]. However, periventricular white matter hyperintense signal did overlap with relatively increased rCTH in one subject (Sub02, see Fig. **2B**), potentially indicating an association between these two markers as has been previously reported [66]. Given that cortical tau pathology can contribute to white matter damage independent of frank FLAIR hyperintense lesions [67], further studies are needed to clarify such associations and the potential role of tau NFT clearance via white matter vasculature.

Moreover, vascular dynamics likely fluctuate throughout the disease course as the cerebral vasculature struggles to maintain oxygen for metabolism with increasing capillary dysfunction. To that end, a longitudinal study in asymptomatic *APOE* ε4 allele carriers showed an inverted U-shape in CBF, with CBF initially increasing to meet the brain's metabolic needs but subsequently decreasing to maximize oxygen availability [68]. Another study showed positive regional correlations between amyloid-β burden and CBF in cognitively normal adults, suggesting a compensatory vascular mechanism early in the disease process [69]. While we provided the amyloid-β status and *APOE* genotype of our cohort subjects when available, we did not examine either factor in the scope of this study. Both amyloid-β oligomers [70] and the *APOE* ε4 allele [71] can disrupt microvascular flow via impaired capillary pericyte function, and further study is needed to disentangle their microvascular effects from those of tau pathology. We also cannot exclude potential vascular contributions of other common AD comorbidities such as Lewy body disease, TDP-43 pathology, and/or small vessel ischemic disease [72].

Strengths of this study include the noninvasive mapping of tau pathology and perfusion arising from the microvasculature in the whole brain using tau-PET and SE-DSC MRI. However, the conclusions of this qualitative study are limited by the small sample size and variable elapsed time between tau-PET and DSC-MRI. Longitudinal studies using Flortaucipir PET suggest that amyloid-negative subjects exhibit minimal cortical tau SUVR change (0-3% increase per year) while amyloid-positive subjects exhibit more pronounced annual tau deposition (3-8% increase per year) [73-76]. Therefore, we cannot exclude the possibility that tau pathology spread to new regions between the Flortaucipir scans and subsequent perfusion MRI in these subjects, particularly those with amyloid-β pathology. Given the cross-sectional nature of this study, the temporal and/or causal relationship(s) between tau accumulation and microvascular function could not be evaluated. Moving forward, longitudinal imaging in a larger subject cohort with cognitively normal controls could better elucidate the specific relationship between tau deposition and microvascular function.

CONCLUSION

In this small case series, complex relationships were observed between tau lesions and microvascular perfusion, with elevated tau uptake associated with variable degrees of CBF reduction and, in some individuals, paradoxically increased CBF. Collectively, the findings present a previously underappreciated heterogeneous relationship between tau and microvascular function that has larger implications for how to monitor therapeutic efficacy in AD. Further study is warranted to better elucidate their interaction in AD pathogenesis and progression.

ETHICS APPROVAL AND CONSENT TO PARTICIPATE

The study was approved by the Massachusetts General Hospital Institutional Review Board [IRB], USA, with the committe number 2020P000370.

HUMAN AND ANIMAL RIGHTS

No animals were used in this study. All the human procedures were followed in accordance with the guidelines of the Declaration of Helsinki.

CONSENT FOR PUBLICATION

All subjects provided written informed consent to participate.

AVAILABILITY OF DATA AND MATERIALS

Not applicable.

FUNDING

This work was supported by the National Institutes of Health, grant numbers P41EB030006, R21AG067562, K99AG061259, and P30AG062421; the Charleston Conference on Alzheimer's Disease New Vision Investigator Award; and the Foundation of the American Society of Neuroradiology's 2020 Boerger Research Fund in Alzheimer's Disease and Neurocognitive Disorders.

CONFLICT OF INTEREST

The authors declare no conflict of interest, financial or otherwise.

ACKNOWLEDGEMENTS

We thank Danielle Mayblyum for organizing and providing clinical, demographic, and neuroimaging summary data. We also thank Dr. Leif Østergaard, Dr. Kim Mouridsen, and Dr. Mikkel Bo Hansen of the Center of Functionally Integrative Neuroscience and MINDLab, Aarhus University, Aarhus, Denmark, for their generous support on the PGUI Perfusion Analysis Software.

REFERENCES

[1] Iturria-Medina Y, Sotero RC, Toussaint PJ, Mateos-Pérez JM, Evans AC, Weiner MW. Early role of vascular dysregulation on late-onset Alzheimer's disease based on multifactorial data-driven analysis. Nat Commun 2016; 7: 11934. http://dx.doi.org/10.1038/ncomms11934 PMID: 27327500

[2] Sweeney MD, Kisler K, Montagne A, Toga AW, Zlokovic BV. The role of brain vasculature in neurodegenerative disorders. Na-

ture Neuroscience. Nature Publishing Group 2018; Vol. 21: pp. 1318-31.

[3] Govindpani K, McNamara LG, Smith NR, Vinnakota C, Waldvogel HJ, Faull RL. Vascular dysfunction in Alzheimer's disease: A prelude to the pathological process or a consequence of it? J Clin Med 2019; 8(5): 651.

[4] Mattsson-Carlgren N, Andersson E, Janelidze S, *et al.* Aβ deposition is associated with increases in soluble and phosphorylated tau that precede a positive Tau PET in Alzheimer's disease. Sci Adv 2020; 6(16): eaaz2387. http://dx.doi.org/10.1126/sciadv.aaz2387 PMID: 32426454

[5] Schöll M, Lockhart SN, Schonhaut DR, *et al.* PET imaging of tau deposition in the aging human brain. Neuron 2016; 89(5): 971-82. http://dx.doi.org/10.1016/j.neuron.2016.01.028 PMID: 26938442

[6] Hanseeuw BJ, Betensky RA, Jacobs HIL, *et al.* Association of amyloid and tau with cognition in preclinical Alzheimer disease: A longitudinal study. JAMA Neurol 2019; 76(8): 915-24. http://dx.doi.org/10.1001/jamaneurol.2019.1424 PMID: 31157827

[7] Malpetti M, Kievit RA, Passamonti L, *et al.* Microglial activation and tau burden predict cognitive decline in Alzheimer's disease. Brain 2020; 143(5): 1588-602. http://dx.doi.org/10.1093/brain/awaa088 PMID: 32380523

[8] Zhao Q, Liu M, Ha L, Zhou Y. Quantitative ^{18}F-AV1451 brain tau PET imaging in cognitively normal older adults, mild cognitive impairment, and Alzheimer's disease patients. Front Neurol 2019; 10(MAY): 486. http://dx.doi.org/10.3389/fneur.2019.00486 PMID: 31156534

[9] Cho H, Choi JY, Hwang MS, *et al.* Tau PET in Alzheimer disease and mild cognitive impairment. Neurology 2016; 87(4): 375-83. http://dx.doi.org/10.1212/WNL.0000000000002892 PMID: 27358341

[10] Park L, Hochrainer K, Hattori Y, *et al.* Tau induces PSD95-neuronal NOS uncoupling and neurovascular dysfunction independent of neurodegeneration. Nat Neurosci 2020; 23(9): 1079-89. http://dx.doi.org/10.1038/s41593-020-0686-7 PMID: 32778793

[11] Bennett RE, Robbins AB, Hu M, *et al.* Tau induces blood vessel abnormalities and angiogenesis-related gene expression in P301L transgenic mice and human Alzheimer's disease. Proc Natl Acad Sci USA 2018; 115(6): E1289-98. http://dx.doi.org/10.1073/pnas.1710329115 PMID: 29358399

[12] Mazzoni MC, Schmid-Schönbein GW. Mechanisms and consequences of cell activation in the microcirculation. Cardiovasc Res 1996; 32(4): 709-19. http://dx.doi.org/10.1016/S0008-6363(96)00146-0 PMID: 8915189

[13] Bullock R, Maxwell WL, Graham DI, Teasdale GM, Adams JH. Glial swelling following human cerebral contusion: An ultrastructural study. J Neurol Neurosurg Psychiatry 1991; 54(5): 427-34. http://dx.doi.org/10.1136/jnnp.54.5.427 PMID: 1865206

[14] Eskildsen SF, Gyldensted L, Nagenthiraja K, *et al.* Increased cortical capillary transit time heterogeneity in Alzheimer's disease: A DSC-MRI perfusion study. Neurobiol Aging 2017; 50: 107-18. http://dx.doi.org/10.1016/j.neurobiolaging.2016.11.004 PMID: 27951412

[15] Nielsen RB, Egefjord L, Angleys H, *et al.* Capillary dysfunction is associated with symptom severity and neurodegeneration in Alzheimer's disease. Alzheimers Dement 2017; 13(10): 1143-53. http://dx.doi.org/10.1016/j.jalz.2017.02.007 PMID: 28343848

[16] Nielsen RB, Parbo P, Ismail R, Dalby R, Tietze A, Brændgaard H. Impaired perfusion and capillary dysfunction in prodromal Alzheimer's disease. Alzheimer's Dement Diagnosis, Assess Dis Monit 2020; 12(1) http://dx.doi.org/10.1002/dad2.12032

[17] Albrecht D, Isenberg AL, Stradford J, *et al.* Associations between vascular function and Tau PET are associated with global cognition and amyloid. J Neurosci 2020; 40(44): 8573-86. http://dx.doi.org/10.1523/JNEUROSCI.1230-20.2020 PMID: 33046556

[18] Nedelska Z, Senjem ML, Przybelski SA, Lesnick TG, Lowe VJ, Boeve BF. Regional cortical perfusion on arterial spin labeling MRI in dementia with Lewy bodies: Associations with clinical severity, glucose metabolism and tau PET. NeuroImage Clin 2018; 19: 939-47.

[19] Visser D, Wolters EE, Verfaillie SCJ, Coomans EM, Timmers T, Tuncel H. Tau pathology and relative cerebral blood flow are independently associated with cognition in Alzheimer's disease. Eur J Nucl Med Mol Imaging 2020; 47(13): 3165-75.

[20] Rubinski A, Tosun D, Franzmeier N, *et al.* Lower cerebral perfusion is associated with tau-PET in the entorhinal cortex across the Alzheimer's continuum. Neurobiol Aging 2021; 102: 111-8. http://dx.doi.org/10.1016/j.neurobiolaging.2021.02.003 PMID: 33765424

[21] Ossenkoppele R, Schonhaut DR, Schöll M, *et al.* Tau PET patterns mirror clinical and neuroanatomical variability in Alzheimer's disease. Brain 2016; 139(Pt 5): 1551-67. http://dx.doi.org/10.1093/brain/aww027 PMID: 26962052

[22] Vogel JW, Young AL, Oxtoby NP, Smith R, Ossenkoppele R, Aksman LM. Spatiotemporal imaging phenotypes of tau pathology in Alzheimer's disease. Alzheimers Dement 2020; 16(S4): e045612. http://dx.doi.org/10.1002/alz.045612

[23] Warkentin S, Ohlsson M, Wollmer P, Edenbrandt L, Minthon L. Regional cerebral blood flow in Alzheimer's disease: classification and analysis of heterogeneity. Dement Geriatr Cogn Disord 2004; 17(3): 207-14. http://dx.doi.org/10.1159/000076358 PMID: 14739546

[24] Jespersen SN, Østergaard L. The roles of cerebral blood flow, capillary transit time heterogeneity, and oxygen tension in brain oxygenation and metabolism. J Cereb Blood Flow Metab 2012; 32(2): 264-77. http://dx.doi.org/10.1038/jcbfm.2011.153 PMID: 22044867

[25] Jiang D, Lin Z, Liu P, *et al.* Brain oxygen extraction is differentially altered by Alzheimer's and vascular diseases. J Magn Reson Imaging 2020; 52(6): 1829-37. http://dx.doi.org/10.1002/jmri.27264 PMID: 32567195

[26] Weisskoff RM, Zuo CS, Boxerman JL, Rosen BR. Microscopic susceptibility variation and transverse relaxation: theory and experiment. Magn Reson Med 1994; 31(6): 601-10. http://dx.doi.org/10.1002/mrm.1910310605 PMID: 8057812

[27] Boxerman JL, Hamberg LM, Rosen BR, Weisskoff RM. MR contrast due to intravascular magnetic susceptibility perturbations. Magn Reson Med 1995; 34(4): 555-66. http://dx.doi.org/10.1002/mrm.1910340412 PMID: 8524024

[28] Folstein MF, Folstein SE, McHugh PR. "Mini-mental state". A practical method for grading the cognitive state of patients for the clinician. J Psychiatr Res 1975; 12(3): 189-98. http://dx.doi.org/10.1016/0022-3956(75)90026-6 PMID: 1202204

[29] Hughes CP, Berg L, Danziger WL, Coben LA, Martin RL. A new clinical scale for the staging of dementia. Br J Psychiatry 1982; 140(6): 566-72. http://dx.doi.org/10.1192/bjp.140.6.566 PMID: 7104545

[30] O'Bryant SE, Waring SC, Cullum CM, Hall J, Lacritz L, Massman PJ. Staging dementia using clinical dementia rating scale sum of boxes scores: A Texas Alzheimer's research consortium study. Arch Neurol 2008; 65(8): 1091-5. http://dx.doi.org/10.1001/archneur.65.8.1091

[31] Nasreddine ZS, Phillips NA, Bédirian V, *et al.* The Montreal Cognitive Assessment, MoCA: A brief screening tool for mild cognitive impairment. J Am Geriatr Soc 2005; 53(4): 695-9. http://dx.doi.org/10.1111/j.1532-5415.2005.53221.x PMID: 15817019

[32] Johnson KA, Schultz A, Betensky RA, Becker JA, Sepulcre J, Rentz D. Tau positron emission tomographic imaging in aging and early Alzheimer disease. Ann Neurol 2016; 79(1): 110-9. http://dx.doi.org/10.1002/ana.24546

[33] Manhard MK, Bilgic B, Liao C, *et al.* Accelerated whole-brain perfusion imaging using a simultaneous multislice spin-echo and gradient-echo sequence with joint virtual coil reconstruction. Magn Reson Med 2019; 82(3): 973-83. http://dx.doi.org/10.1002/mrm.27784 PMID: 31069861

[34] Li X, Wang D, Auerbach EJ, Moeller S, Ugurbil K, Metzger GJ. Theoretical and experimental evaluation of multi-band EPI for high-resolution whole brain pCASL Imaging. Neuroimage 2015; 106: 170-81. http://dx.doi.org/10.1016/j.neuroimage.2014.10.029

[35] Cox RW, Jesmanowicz A. Real-time 3D image registration for

functional MRI. Magn Reson Med 1999; 42(6): 1014-8. http://dx.doi.org/10.1002/(SICI)1522-2594(199912)42:6<1014::AID-MRM4>3.0.CO;2-F PMID: 10571921

[36] Chappell MA, Groves AR, Whitcher B, Woolrich MW. Variational Bayesian inference for a nonlinear forward model. IEEE Trans Signal Process 2009; 57(1): 223-36. http://dx.doi.org/10.1109/TSP.2008.2005752

[37] Ishii K, Sasaki M, Matsui M, *et al.* A diagnostic method for suspected Alzheimer's disease using H(2)15O positron emission tomography perfusion Z score. Neuroradiology 2000; 42(11): 787-94. http://dx.doi.org/10.1007/s002340000404 PMID: 11151682

[38] Johnson NA, Jahng GH, Weiner MW, *et al.* Pattern of cerebral hypoperfusion in Alzheimer disease and mild cognitive impairment measured with arterial spin-labeling MR imaging: initial experience. Radiology 2005; 234(3): 851-9. http://dx.doi.org/10.1148/radiol.2343040197 PMID: 15734937

[39] Schuff NW, Du A-T, Jahng G, Mueller S, Stables L, Cashdollar N. Regional decline of brain perfusion in healthy aging detected with arterial spin labeling at 4T. Alzheimers Dement 2005; 1: S83-3. http://dx.doi.org/10.1016/j.jalz.2005.06.293

[40] Du AT, Jahng GH, Hayasaka S, *et al.* Hypoperfusion in frontotemporal dementia and Alzheimer disease by arterial spin labeling MRI. Neurology 2006; 67(7): 1215-20. http://dx.doi.org/10.1212/01.wnl.0000238163.71349.78 PMID: 17030755

[41] Yoshiura T, Hiwatashi A, Noguchi T, *et al.* Arterial spin labelling at 3-T MR imaging for detection of individuals with Alzheimer's disease. Eur Radiol 2009; 19(12): 2819-25. http://dx.doi.org/10.1007/s00330-009-1511-6 PMID: 19588145

[42] Chen Y, Wolk DA, Reddin JS, *et al.* Voxel-level comparison of arterial spin-labeled perfusion MRI and FDG-PET in Alzheimer disease. Neurology 2011; 77(22): 1977-85. http://dx.doi.org/10.1212/WNL.0b013e31823a0ef7 PMID: 22094481

[43] Dashjamts T, Yoshiura T, Hiwatashi A, *et al.* Simultaneous arterial spin labeling cerebral blood flow and morphological assessments for detection of Alzheimer's disease. Acad Radiol 2011; 18(12): 1492-9. http://dx.doi.org/10.1016/j.acra.2011.07.015 PMID: 21907599

[44] Kobayashi R, Hayashi H, Kawakatsu S, Okamura N, Yoshioka M, Otani K. Assessment of amyloid deposition in patients with probable REM sleep behavior disorder as a prodromal symptom of dementia with lewy bodies using PiB-PET. Front Neurol 2019; 10: 671. http://dx.doi.org/10.3389/fneur.2019.00671 PMID: 31293508

[45] Daniela P, Orazio S, Alessandro P, Mariano NF, Leonardo I, Pasquale Anthony DR. A survey of FDG- and amyloid-PET imaging in dementia and grade analysis. BioMed Res Intern Hindawi Lim 2014; 2014: p. 785039.

[46] Ciarmiello A, Tartaglione A, Giovannini E, *et al.* Amyloid burden identifies neuropsychological phenotypes at increased risk of progression to Alzheimer's disease in mild cognitive impairment patients. Eur J Nucl Med Mol Imaging 2019; 46(2): 288-96. http://dx.doi.org/10.1007/s00259-018-4149-2 PMID: 30244387

[47] Postelnicu G, Zollei L, Fischl B. Combined volumetric and surface registration. IEEE Trans Med Imaging 2009; 28(4): 508-22. http://dx.doi.org/10.1109/TMI.2008.2004426

[48] Zöllei L, Stevens A, Huber K, Kakunoori S, Fischl B. Improved tractography alignment using combined volumetric and surface registration. Neuroimage 2010; 51(1): 206-13. http://dx.doi.org/10.1016/j.neuroimage.2010.01.101 PMID: 20153833

[49] Gao JS, Huth AG, Lescroart MD, Gallant JL. Pycortex: An interactive surface visualizer for fMRI. Front Neuroinform 2015; 9: 23. http://dx.doi.org/10.3389/fninf.2015.00023 PMID: 26483666

[50] Albert MS, DeKosky ST, Dickson D, *et al.* The diagnosis of mild cognitive impairment due to Alzheimer's disease: recommendations from the National Institute on Aging-Alzheimer's Association workgroups on diagnostic guidelines for Alzheimer's disease. Alzheimers Dement 2011; 7(3): 270-9. http://dx.doi.org/10.1016/j.jalz.2011.03.008 PMID: 21514249

[51] McKhann GM, Knopman DS, Chertkow H, *et al.* The diagnosis of dementia due to Alzheimer's disease: recommendations from the National Institute on Aging-Alzheimer's Association workgroups on diagnostic guidelines for Alzheimer's disease. Alzheimers Dement 2011; 7(3): 263-9. http://dx.doi.org/10.1016/j.jalz.2011.03.005 PMID: 21514250

[52] Crary JF, Trojanowski JQ, Schneider JA, *et al.* Primary age-related tauopathy (PART): A common pathology associated with human aging. Acta Neuropathol 2014; 128(6): 755-66. http://dx.doi.org/10.1007/s00401-014-1349-0 PMID: 25348064

[53] van de Haar HJ, Jansen JFA, van Osch MJP, *et al.* Neurovascular unit impairment in early Alzheimer's disease measured with magnetic resonance imaging. Neurobiol Aging 2016; 45: 190-6. http://dx.doi.org/10.1016/j.neurobiolaging.2016.06.006 PMID: 27459939

[54] van Beek AHEA, Lagro J, Olde-Rikkert MGM, Zhang R, Claassen JAHR. Oscillations in cerebral blood flow and cortical oxygenation in Alzheimer's disease. Neurobiol Aging 2012; 33(2): 428.e21-31. http://dx.doi.org/10.1016/j.neurobiolaging.2010.11.016 PMID: 21208686

[55] Asllani I, Habeck C, Scarmeas N, Borogovac A, Brown TR, Stern Y. Multivariate and univariate analysis of continuous arterial spin labeling perfusion MRI in Alzheimer's disease. J Cereb Blood Flow Metab 2008; 28(4): 725-36. http://dx.doi.org/10.1038/sj.jcbfm.9600570 PMID: 17960142

[56] Kogure D, Matsuda H, Ohnishi T, Asada T, Uno M, Kunihiro T. Longitudinal Evaluation of Early Alzheimer's Disease Using Brain Perfusion SPECT. J Nuc Med 2000; 14(7): 1155-62.

[57] Leeuwis AE, Benedictus MR, Kuijer JPA, *et al.* Lower cerebral blood flow is associated with impairment in multiple cognitive domains in Alzheimer's disease. Alzheimers Dement 2017; 13(5): 531-40. http://dx.doi.org/10.1016/j.jalz.2016.08.013 PMID: 27693109

[58] Braak H, Braak E. Neuropathological stageing of Alzheimer-related changes. Acta Neuropathol 1991; 82(4): 239-59. http://dx.doi.org/10.1007/BF00308809 PMID: 1759558

[59] Schwarz AJ, Yu P, Miller BB, *et al.* Regional profiles of the candidate tau PET ligand 18F-AV-1451 recapitulate key features of Braak histopathological stages. Brain 2016; 139(Pt 5): 1539-50. http://dx.doi.org/10.1093/brain/aww023 PMID: 26936940

[60] Franzmeier N, Dewenter A, Frontzkowski L, *et al.* Patient-centered connectivity-based prediction of tau pathology spread in Alzheimer's disease. Sci Adv 2020; 6(48): eabd1327. http://dx.doi.org/10.1126/sciadv.abd1327 PMID: 33246962

[61] Yamauchi H, Kagawa S, Takahashi M, Oishi N, Ono M, Higashi T. Misery perfusion and amyloid deposition in atherosclerotic major cerebral artery disease. NeuroImage Clin 2019; 22: 101762. http://dx.doi.org/10.1016/j.nicl.2019.101762

[62] Matsumoto Y, Ogasawara K, Saito H, *et al.* Detection of misery perfusion in the cerebral hemisphere with chronic unilateral major cerebral artery steno-occlusive disease using crossed cerebellar hypoperfusion: comparison of brain SPECT and PET imaging. Eur J Nucl Med Mol Imaging 2013; 40(10): 1573-81. http://dx.doi.org/10.1007/s00259-013-2463-2 PMID: 23740375

[63] Nagata K, Buchan RJ, Yokoyama E, Kondoh Y, Sato M, Terashi H. Misery perfusion with preserved vascular reactivity in Alzheimer's disease. Ann N Y Acad Sci 1997; 826: 272-81.

[64] Wardlaw JM, Smith EE, Biessels GJ, Cordonnier C, Fazekas F, Frayne R. Neuroimaging standards for research into small vessel disease and its contribution to ageing and neurodegeneration.The Lancet Neurology. Elsevier 2013; pp. 822-32. http://dx.doi.org/10.1016/S1474-4422(13)70124-8

[65] Pantoni L. Cerebral small vessel disease: from pathogenesis and clinical characteristics to therapeutic challenges. Lancet Neurol 2010; 9(7): 689-701. http://dx.doi.org/10.1016/S1474-4422(10)70104-6 PMID: 20610345

[66] Dalby RB, Eskildsen SF, Videbech P, *et al.* Oxygenation differs among white matter hyperintensities, intersected fiber tracts and unaffected white matter. Brain Commun 2019; 1(1): fcz033. http://dx.doi.org/10.1093/braincomms/fcz033 PMID: 32954272

[67] Strain JF, Smith RX, Beaumont H, Roe CM, Gordon BA, Mishra

S. Loss of white matter integrity reflects tau accumulation in Alzheimer disease defined regions. Neurology 2018; 91(4): E313-8.
http://dx.doi.org/10.1212/WNL.0000000000005864

[68] Thambisetty M, Beason-Held L, An Y, Kraut MA, Resnick SM. APOE ε4 genotype and longitudinal changes in cerebral blood flow in normal aging. Arch Neurol 2010; 67(1): 93-8.
http://dx.doi.org/10.1001/archneurol.2009.913 PMID: 20065135

[69] Fazlollahi A, Calamante F, Liang X, *et al.* Increased cerebral blood flow with increased amyloid burden in the preclinical phase of alzheimer's disease. J Magn Reson Imaging 2020; 51(2): 505-13.
http://dx.doi.org/10.1002/jmri.26810 PMID: 31145515

[70] Nortley R, Korte N, Izquierdo P, Hirunpattarasilp C, Mishra A, Jaunmuktane Z. Amyloid b oligomers constrict human capillaries in Alzheimer's disease *via* signaling to pericytes. Science 2019; 365(6450): eaav9518.
http://dx.doi.org/10.1126/science.aav9518

[71] Montagne A, Nation DA, Sagare AP, *et al.* APOE4 leads to blood--brain barrier dysfunction predicting cognitive decline. Nature 2020; 581(7806): 71-6.
http://dx.doi.org/10.1038/s41586-020-2247-3 PMID: 32376954

[72] Spina S, La Joie R, Petersen C, Nolan AL, Cuevas D, Cosme C. Comorbid neuropathological diagnoses in early *versus* late-onset Alzheimer's disease. Brain 2021; 144(7): 2186-98.

[73] Harrison TM, La Joie R, Maass A, Baker SL, Swinnerton K, Fenton L. Longitudinal tau accumulation and atrophy in aging and alzheimer disease. Ann Neurol 2019; 85(2): 229-40.
http://dx.doi.org/10.1002/ana.25406

[74] Jack CR Jr, Wiste HJ, Schwarz CG, *et al.* Longitudinal tau PET in ageing and Alzheimer's disease. Brain 2018; 141(5): 1517-28.
http://dx.doi.org/10.1093/brain/awy059 PMID: 29538647

[75] Pontecorvo MJ, Devous MD, Kennedy I, *et al.* A multicentre longitudinal study of flortaucipir (18F) in normal ageing, mild cognitive impairment and Alzheimer's disease dementia. Brain 2019; 142(6): 1723-35.
http://dx.doi.org/10.1093/brain/awz090 PMID: 31009046

[76] Cho H, Choi JY, Lee HS, *et al.* Progressive tau accumulation in Alzheimer disease: 2-year follow-up study. J Nucl Med 2019; 60(11): 1611-21.
http://dx.doi.org/10.2967/jnumed.118.221697 PMID: 30926651